Dynamic genome-scale modeling of *Saccharomyces cerevisiae* unravels mechanisms for higher alcohol and ester formation during alcoholic fermentation

William T. Scott, Jr.[1,2,3]*, David Henriques[4]*, Eddy J. Smid[3], Richard A. Notebaart[3], and Eva Balsa-Canto[4]

[1]UNLOCK Large Scale Infrastructure for Microbial Communities, Wageningen University & Research, Wageningen, The Netherlands

[2]Laboratory of Systems and Synthetic Biology, Wageningen University & Research, Wageningen, The Netherlands

[3]Food Microbiology, Wageningen University & Research, Wageningen, The Netherlands

[4](Bio)process Engineering Group, IIM-CSIC, Vigo, Spain

*Address correspondence to william.scott@wur.nl and davidh@iim.csic.es

Postal Address:
Wageningen University & Research
Laboratory of Systems and Synthetic Biology
Stippeneng 4
Building 124 (Helix)
6708 WE Wageningen

ORCID: William T. Scott, Jr. - https://orcid.org/0000-0002-4029-2998, David Henriques - https://orcid.org/0000-0002-9477-292X, Eddy J. Smid - https://orcid.org/0000-0002-6687-5083, Richard A. Notebaart - https://orcid.org/0000-0003-3469-1893, and Eva Balsa-Canto - https://orcid.org/0000-0002-1978-2626

Running Title: Higher alcohol and ester formation during fermentation

SUMMARY

Fermentation employing *Saccharomyces cerevisiae* has produced alcoholic beverages and bread for millennia. More recently, *S. cerevisiae* has been used to manufacture specific metabolites for the food, pharmaceutical, and cosmetic industries. Among the most important of these metabolites are compounds associated with desirable aromas and flavors, including higher alcohols and esters. While the physiology of yeast has been well-studied, its metabolic modulation leading to aroma production under industrial relevant scenarios such as winemaking is still unclear. Furthermore, what are the underlying metabolic mechanisms explaining the conserved and varying behavior of yeasts regarding aroma formation under enological conditions? Dynamic flux balance analysis (dFBA) was employed to answer these questions using the latest genome-scale metabolic model (GEM) of *S. cerevisiae*. Although we found several conserved mechanisms among wine yeasts, e.g., acetate ester formation is dependent on intracellular metabolic acetyl-CoA/CoA levels, and the formation of ethyl esters facilitates the removal of toxic fatty acid from cells using CoA, species-specific mechanisms were also found, e.g., carbohydrate accumulation induces redox restrictions later for strain Uvaferm. In conclusion, our new metabolic model of yeast under enological conditions revealed key metabolic mechanisms in wine yeasts, which will aid future research strategies to optimize their behavior in industrial settings.

KEYWORDS: Dynamic flux balance analysis (dFBA), Metabolic modeling, Wine, Fermentation, Yeast, Higher alcohols, Esters

INTRODUCTION

The genetics and metabolism of the yeast, *Saccharomyces cerevisiae*, have been studied extensively as a model eukaryotic organism (Botstein et al., 1997). However, despite its general use for industrial processes such as winemaking, variability in fermentation performance, especially in growth and aroma production, is not entirely understood (Hirst and Richter, 2016). Since prominent aromas, e.g., higher alcohols and esters, are partially produced during active growth, factors that impact yeast growth simultaneously influence essential aroma formation (Dekoninck, 2012). Furthermore, commercial yeast strains vary by orders of magnitude in their aroma production (Gonzalez and Morales, 2017, Pérez et al., 2021). This variation is associated with a myriad of genetic (Peter et al., 2018) and environmental factors such as nitrogen and micronutrients concentration levels (Su et al., 2021), temperature (Rollero et al., 2015), pH (Lam et al., 2014), ethanol concentration levels (Snoek et al., 2016), and the presence of toxins (Viegas et al., 1989). However, commercial strains of wine yeast respond to these factors differently in poorly understood ways, but seem to be correlated with specific parts of yeast metabolism, such as those involved in lipid formation and membrane composition (Henderson et al., 2013).

Moreover, particular aromas are suggested to be synthesized because of the detoxification of medium-chain fatty acids. It is also speculated that aroma formation is part of a metabolic process used to balance the acetyl-CoA/CoA ratio (Mason and Dufour, 2000). Understanding the difference in metabolism in yeast strains will lead to a greater ability to control and manipulate aroma-related performance. That greater metabolic understanding will facilitate insight into the specific mechanisms inducing aroma formation.

It is advantageous to take a systems biology approach to comprehensively understand these differences in yeast metabolism. Several studies have examined yeast volatile organic compound (VOC) or aroma production (Miller et al., 2007, Seguinot et al., 2018). Some of these studies have

combined omics approaches, exploring the link between yeast gene expression and metabolomics (Dunn et al., 2005) or analyzing the transcriptome and metabolome profiles of yeast strains to assess the expressed genes on aroma formation during wine fermentation (Rossouw et al., 2008). Although there is experimental evidence for differences in the metabolism of various strains and genes involved in aroma formation, these experimentally-derived large data sets can be challenging to generate and analyze, especially in terms of finding the most important differences relevant to the metabolism being studied. As an alternative, mathematical modeling of yeast metabolism can provide a more comprehensive means to examine how yeast metabolism changes during the entire course of wine fermentation and which parts of overall metabolism are interrelated.

Metabolic modeling of yeast under enological conditions has been reported for some time (Boulton, 1980, Cramer et al., 2002, Sainz et al., 2003, Pizarro et al., 2007). The general approach has been to use Flux Balance Analysis (FBA) with a subset of metabolites and metabolic reactions found in yeast during alcoholic fermentation (Quiros et al., 2013), often augmented to dynamic FBA (dFBA) to account for the time-dependent nature of wine fermentations and their associated yeast metabolism. More recently, the number of metabolites and reactions included in models of *Saccharomyces cerevisiae* has grown to be more comprehensive to the point where they are often referred to as genome-scale metabolic models (GEMs). The prior application of dFBA to less extensive GEMs for studying wine fermentations (Vargas et al., 2011); however, that study lacked exploration into intracellular flux behavior and insight into how kinetic constraints impact prediction performance. Consensus GEMs for yeast have developed from model iFF708 (Forster et al., 2003) to increasingly comprehensive models (Nookaew et al., 2008, Aung et al., 2013), with the newest consensus model being Yeast8 (Lu et al., 2019). This recent model has been further

curated to include some lipid synthesis pathways and amino acid degradation pathways to account for the production of higher alcohols, carboxylic, acids and esters (Scott et al., 2020), which have been proven to be key in imparting desirable aromas to alcoholic beverages (for more details, see review by (Dzialo et al., 2017)). Yeast8 has been combined with constraint-based modeling approaches to understand yeast metabolism in a few studies. However, the use of this yeast GEM has thus far been confined to glucose-limited, aerobic conditions (Moreno-Paz et al., 2022), nutrient-rich cases (Henriques et al., 2021b) and/or under non-transient model scenarios (Scott et al., 2021b), thus limiting its scope and applicability to accurately predict enological conditions.

In this study, the Yeast8.5.0 GEM (Lu et al., 2019), along with the dFBA framework (Henriques et al., 2021b), were employed to predict the metabolic behavior of *Saccharomyces cerevisiae* under enological conditions. The model was mainly used to model nitrogen-limited, anaerobic growth of *S. cerevisiae* with appropriate kinetic constraints, and utilizing a biomass equation tailored for enological conditions. After validating the model predictions with published experimental data from four commercial yeast strains (Scott et al., 2021a), a goodness of fit of the model predictions was assessed for each strain to evaluate the accuracy and quality of the model predictions. From our model simulations, conserved behavior was identified across the strains. In particular, higher alcohols maintain redox homeostasis during the carbohydrate accumulation phase, acetate ester formation depends on intracellular metabolic acetyl-CoA/CoA levels, and the formation of ethyl esters facilitates the removal of toxic fatty acid from cells using CoA. However, some strain-specific mechanisms were noticed, such as strain behavior varied notably during the carbohydrate accumulation phase, carbohydrate accumulation induced NAD+/NADH restrictions later for the Uvaferm strain, and the Opale strain preferred the shikimate pathway, which led to more 2-phenylethanol production than the other strains.

RESULTS AND DISCUSSION

Multi-phase multi-objective dynamic flux balance analysis framework

We adapted the model described in (Henriques, et al., 2021) to describe the intracellular fluxes. Here, we divided the process into five phases in which cellular objectives and flux constraints must be adapted: lag, exponential growth, carbohydrate accumulation, stationary, and decay (see Fig. 1). The duration of the phases was determined by the parameters t_L, t_E, t_s, and t_D.

Previously, the model relied on a dynamic biomass equation dependent on the amount of YAN in the medium. Nevertheless, this equation required the estimation of several parameters without information about biomass composition (protein, mRNA, carbohydrates). In addition, the model could not accurately explain the observed behavior of the non-*cerevisiae* species (Uvaferm). This strain presented a long growth period with virtually no nitrogen sources available. To address this, we replaced the phase previously known as growth under nitrogen limitation with the carbohydrate accumulation phase (see (Henriques et al., 2021a)) in the previously published model.

Most of the other nitrogen sources were consumed primarily during the exponential growth phase, except glycine. In this period, the cellular objective was the maximization of biomass. In contrast with the previous model, during carbohydrate accumulation (previously growth under nitrogen limitation), the cellular objective of protein maximization and the procedure to simulate protein turnover (described in (Henriques et al., 2021b)) were activated. Also, to simulate carbohydrate accumulation, during this period, an exchange flux for this compound (s_3717[c]) was added to the stoichiometric network determined by the equation:

$$v_{carb} = \tau_{Carb} \cdot \left(\theta_{Carb} - \frac{X_{Carb}}{X}\right),$$

where X_{Carb}(g/L) is the carbohydrate quantity present in the biomass, X is the biomass (g/L), θ_{Carb} is the final carbohydrate content and τ_{Carb} is the parameter controlling the convergence speed towards θ_{Carb} (see complete equations in supplementary code example (dynamic genome-scale modeling of yeast fermentation): https://sites.google.com/site/amigo2toolbox/examples).

Higher alcohol production can occur due to assimilation/catabolism of amino acids or *de novo* synthesis. The previous model considered that higher alcohol production started during growth under nitrogen limitation and was prolonged through the stationary phase. The experiments considered in that work included ammonium diphosphate supplementation, and the final concentrations of higher alcohols were higher than those reported here. Here, the relative contributions of higher alcohols produced during the first hours of growth were relevant. Thus, to account for this effect, during exponential growth, we set the production of isoamyl alcohol, 2-phenyl ethanol, and isobutanol at the same flux as the consumption of the corresponding amino acids (leucine, phenylalanine, and isoleucine).

Validation and goodness of fit of the model predictions against enological fermentation data

This study employed data from experimental fermentations carried out under enological conditions (see (Scott et al., 2021a)). The model profiles of the four strains for glucose and fructose uptake, and the secretion of ethanol, acetate, malate, succinate, and glycerol, are depicted throughout the fermentation (Fig. 2). The nitrogen consumed by the yeast was in the form of amino acids and ammonium in the MMM synthetic grape medium, and the model profiles for the nitrogen sources for the four strains are shown (Fig. 3). As expected, since it has been well documented that wine fermentations are nitrogen-limited as suggested in several studies (Ingledew and Kunkee, 1985, Cramer et al., 2002, Varela et al., 2004), the yeast assimilable nitrogen (YAN) (a measure of the concentration of all nitrogen in the free amino acids and ammonium) was consumed very

rapidly. At that point, the maximum cell density was reached. The dFBA analysis also accurately simulated the profiles of several important VOCs for the four strains (Fig. 4).

The final model contained 50 ODEs, consisting of 60 parameters determined from time-course data for all measured extracellular metabolites and biomass. For the primary metabolites, as shown, glucose in the medium was consumed first, followed by fructose since hexose transporters in the cytoplasm have a higher affinity for the former (Fig. 2). A stoichiometrically accurate yield of ethanol (~101 g/L) was predicted for the strains, reaching an average simulated concentration of 100 g/L with the initial starting concentration of total sugar used in this study (~220 g/L) (Fig. 2). Moreover, the values were within the range of similar enological fermentations (Ribéreau-Gayon et al., 2000). Various other essential extracellular metabolites are also measured and predicted throughout fermentation (Fig. 2), including glycerol, malate, succinate, and acetate, with average yields among strains of ~7 g/L, ~3.2 g/L, ~1.4 g/L, and ~0.5 g/L, respectively.

Consumption of glucose and fructose, and production of ethanol simulations were representative of the enological conditions achieving excellent fits against the experimental dynamic profiles (with median R^2 values of 0.98, 0.96, and 0.98 among the strains) (see Fig. 2 and Table S1). YAN and biomass (dry cell weight) curves were also successfully predicted for all the strains, where the median R^2 values among the strains are 0.92 and 0.96, respectively (see Table S1). In addition, the production of some of the important by-products of wine fermentation, including glycerol, succinate, and acetate, were successfully simulated by the model achieving moderately good fits among the strains with median R^2 values of 0.89, 0.81, and 0.77 (Fig. 2 and Table S1). Maximum glycerol (~6.9 g/L) and succinate (~1.3 g/L) produced during the fermentation were quantitatively well predicted using the model, while acetate (~0.5 g/L) prediction was reasonably good (Fig. 2).

For the consumption of nitrogenous compounds including amino acids the model simulations obtained excellent fits against experimental data with each of the amino acid dynamic profiles containing a median $R^2 > 0.92$ except for histidine (0.83), lysine (0.80), and asparagine (0.79). The model also simulated kinetic curves that were in moderate agreement with experimental data for the VOCs for most strains which have $R^2 > 0.85$ (see Table S1). However, some strains contain less decent fits for a few VOCs e.g., ethyl hexanoate (Table S1 and Fig. S2). For instance, there was only a slight underprediction of propanol for the Uvaferm strain (see Fig. 3).

Predictions of key intracellular fluxes across different cell growth phases

Using *Yeast 8.5.0* combined with our dFBA model framework, it is possible to predict the change of the entire set of fluxes throughout the simulated fermentation. The dynamic flux ratios of some of the key intracellular fluxes between 6 to 40 hours during fermentation (carbohydrate accumulation phase) are illustrated (Fig. S1). However, essential fluxes concerning an anaerobic nitrogen-limited yeast phenotype were observed in all growth phases (see supplementary data text files). These fluxes pertained to portions of central carbon, nitrogen, and lipid metabolism. This key set of fluxes includes presenting the role of NAD-dependent acetaldehyde dehydrogenase (r_2115) to restore redox balance and permit the anaerobic growth at differing levels among the strains as shown previously (Vargas et al., 2011, Scott et al., 2021b). Moreover, the simulations pointed to many of the same reaction fluxes such as aspartate -semialdehyde dehydrogenase (6.33×10^{-4}, 1.05×10^{-3}, 1.22×10^{-4}, and 9.36×10^{-4} mmol/mmolH for Opale, R2, Elixir, and Uvaferm respectively), homoserine dehydrogenase (6.33×10^{-4}, 1.05×10^{-3}, 1.22×10^{-4}, and 9.36×10^{-4} mmol/mmolH for Opale, R2, Elixir, and Uvaferm respectively) , and glycerol-3-phosphate

dehydrogenase (7.10 x 10^{-2}, 8.00 x 10^{-2}, 6.31 x 10^{-2}, and 7.95 x 10^{-2} mmol/mmolH for Opale, R2, Elixir, and Uvaferm, respectively) (where mmolH is millimoles of consumed hexose x 100) responsible for strain-dependent behavior as demonstrated in recent studies (Henriques et al., 2021b, Scott et al., 2021b). This result underscores the tight link between glycolysis, the TCA cycle, and amino acid metabolism under nitrogen-limited conditions.

Strain behavior varied notably during the carbohydrate accumulation phase

When examining the dynamic concentration profiles, the most apparent variation among the strains corresponds to extracellular metabolites associated with core carbon, nitrogen, and lipid metabolism. These notable differences are evident when observing the secretion dynamics of acetate, glycerol, and succinate (Fig. 2) as well as the overall production of many VOCs, e.g., propanol, isoamylol, isobutanol, isoamyl acetate, phenylethyl acetate, and ethyl butanoate (Fig. 3 and Fig. 4).

The model framework was employed to elucidate the metabolic mechanisms adopted by the strains to achieve different compound concentration levels. The dynamic flux ratios were determined using the aforementioned equations. Dynamic flux ratios which were determined for each phase and the entire fermentation, are reported (see Fig. S1). The observed variation in dynamic flux ratios among the strains across growth phases is summarized in the supplement.

Although Uvaferm strain experienced substantial flux in many reactions associated with redox balance and acetyl CoA during the stationary phase, the intracellular behavior differs among the strains most significantly during the carbohydrate accumulation phase. The exponential and carbohydrate accumulation phase also coincides with the vigorous production of higher alcohols and esters desirable in fermented beverages such as wine and beer and commercially crucial for

fragrances (for more info see Fig. S1 and S2). For instance, isoamyl acetate known for producing fruity aromas, experienced predicted dynamic flux ratios of 6.5 x 10-5, 5.3 x 10-5, 6.5 x 10-5, and 6.8 x 10-5 mmol/mmolH during the exponential and carbohydrate acc. phases whereas during stationary phase the Uvaferm strain was the only strain to experience a flux which was 6.8 x 10-5 mmol/mmolH. Therefore, the following sections expound on metabolic effects during the carbohydrate accumulation phase.

Carbohydrate accumulation induces NAD+/NADH restrictions later for strain Uvaferm

The model predictions for growth were similar among the strains except for the Uvaferm strain, which experienced a later onset of stationary phase (150 h) compared to other strains (80 h) (Table S1). Under nitrogen-limited fermentation conditions, sluggish fermentation can occur due to lower relative protein turnover, resulting in higher relative amounts of RNA and storage carbohydrates, e.g., trehalose (Varela et al., 2004). Furthermore, the release of C6 sugars from trehalose and glycogen mainly occurs during the onset of the stationary phase (Nissen et al., 1997). For the strains in this study excluding the Uvaferm, this release was predicted to occur at the carb. accumulation phase Uvaferm showed comparably lower flux values for both the carbohydrate pseudo-reaction (r_4048: dynamic flux ratio = 8.51 x 10^{-3} mmol/mmolH) and trehalose-phosphatase (r_1051: dynamic flux ratio = 1.18 x 10^{-3} mmol/mmolH). However, Uvaferm was the only strain to have flux for both reactions during the stationary phase. This particularity suggests intracellular mechanisms bring about carbohydrate storage or accumulation for the other strains or later for Uvaferm.

As nitrogen limitation conditions arise, yeast metabolism circulates more sugar flux into the fermentation. As such, there is a decline in cell growth, and what is not spent (sugar, nitrogen, etc., flux) on biomass synthesis is directed to other routes. Overall, for Uvaferm, the decline in

protein synthesis and lipid production lowered the demand for NADPH (see fluxes Table S2). At the onset of carbohydrate accumulation due to nitrogen limitation, restriction of NAD+ occurred. As nitrogen limits the rate of glucose and fructose uptake in conjunction with growth, the model opted to employ the glyoxylate cycle to reduce NADH production while still producing necessary tricarboxylic acid (TCA) cycle intermediates (Fig. 2).

Yeast cells produced most of the succinate during the carbon accumulation phase, where the Uvaferm strain contained a higher dynamic flux ratio than the other strains (Table S3). This higher succinate concentration in Uvaferm is caused by cells taking up a preferred nitrogen source, i.e., glutamate, which becomes deaminated by NAD+ dependent glutamate dehydrogenase to discharge α-ketoglutarate and ammonium (Fig. 3). Consequently, the increase in the intracellular α- ketoglutarate concentration increases enzyme activities of the oxidative branch of the TCA cycle, causing succinate production. Previous works have alluded to the fact that carbon skeletons derived from deaminated glutamate are easily facilitated into the TCA cycle and, hence, transformed into succinate (Tesnière et al., 2015). This premise is supported by the model, which uses an aspartate transaminase-associated reaction (r_0216) to link glutamate and thus steer succinate formation (Fig. 3).

Production of higher alcohols maintains redox homeostasis at the carb. accumulation phase

Higher alcohols are quantitatively the most abundant VOCs produced by yeasts. These higher alcohols and their respective acetate esters are produced predominantly via the Ehrlich pathway (Ehrlich, 1907, Hazelwood et al., 2008) or *de novo* synthesis routes (Gonzalez and Morales, 2017). Higher alcohols have been shown to be produced through this route to regenerate NADH and preserve the redox balance in yeast cells (Lambrechts and Pretorius, 2000, Jain et al.,

2012, Henriques et al., 2021b). The Ehrlich pathway consists of three steps: a transamination step, a decarboxylation step, and a reduction step. At the reduction step, one of two paths can be taken by fusel aldehydes: either an oxidation route using an *ALD* to respective fusel acids or a reduction step via *ADH*s and *AAD*s to catalyze the production of the respective higher alcohols. This route is seen when examining reactions (r_0171, r_0181, and r_0184) to synthesize 2-phenylethanol (PEA), isoamylol, and isobutanol, respectively. Opale produced the most significant amount of higher alcohol among the strains. In particular, the Opale strain dynamic flux ratios for higher alcohols amounted to 2.42 mmol/mmolH during the carbohydrate accumulation phase.

Over the course of the exponential growth phase, the model predicted a vigorous formation of higher alcohols that were produced via amino acid degradation routes (Ehrlich pathway). However, during the carbohydrate accumulation phase, our model simulated most significant higher alcohols are formed from the Ehrlich pathway and *de novo* synthesis routes. It also showed sharp increases in flux values from the exponential phase (Fig. 4). Furthermore, our model analysis indicated that the *de novo* synthesis pathways rather than the Ehrlich pathway from central carbon metabolism were responsible for forming isoamyl alcohol and isobutanol. More specifically, these higher alcohols were produced from glycolytic, and pentose phosphate pathway (PPP) intermediates preferentially to the amino acid degradation pathways (leucine and valine, respectively) (Fig. 4). This result agrees with some recent studies that have shown using carbon tracer experiments (Nisbet et al., 2014, Crépin et al., 2017) and metabolic modeling (Quiros et al., 2013, Henriques et al., 2021b) that higher alcohol formation is influenced more via the anabolic pathways from central carbon metabolism. The differences in strain behavior seen here could be due to how nitrogen limitation or carbohydrate accumulation impacts redox states through the

demand for ATP, NAD, and NADPH cofactors or strain-dependent nitrogen requirements (Albers et al., 1996).

Pyruvate in the mitochondrion took two different routes: acetyl-CoA (r_0961: 1.8 x 10^{-4}, 8.3 x 10^{-5}, 2.8 x 10^{-5}, and 6.7 x 10^{-4} mmol/mmolH for Opale, R2, Elixir, and Uvaferm, respectively) and 2-acetyllactic acid (r_0097: 0, 0, 0, and 1.4 x 10^{-3} mmol/mmolH for Opale, R2, Elixir, and Uvaferm, respectively). It was observed during the stationary phase; that the Uvaferm strain utilized the carnitine shuttle (r_0254) to generate acetyl-CoA the most compared with other strains. Then, 2-acetyllactic acid proceeded to be converted to 3- methyl-2-oxobutanoate, consuming one NADPH (r_0096), which presented two divergent routes: the production of 2-isopropylmalate (concluding with isoamyl alcohol; r_0025, r_0072, and r_0179) or valine (ending with the formation of isobutanol via the Ehrlich pathway; r_1087, r_0062, and r _0182). Throughout this process, Uvaferm achieved relatively higher flux values (at least 2-fold greater) than the other strains.

Opale strain shows a more effective production of PEA by utilizing the shikimate pathway

PEA production via the Ehrlich pathway involves three steps: a transamination step (r_2117) to form the α-keto-phenylpyruvate, a decarboxylation step (r_0854) to form phenylacetaldehyde followed by a reduction step (r_0171) to form the higher alcohol (PEA). Subsequently, PEA reacts with acetyl-CoA to form an ester, 2-phenylacetate (Dzialo et al., 2017). Overall, the Opale strain produced the most PEA (Fig. 3). The model indicated that this enhanced PEA production in the Opale strain was caused by higher flux diverted through the shikimate pathway (r_0996 and r_0279) (Fig. 4).

The shikimate pathway is a convenient pathway for the biosynthesis of several aromatic compounds, including PEA. This route initially involves the condensation of phosphoenolpyruvate (PEP, stemming from the glycolysis pathway) (r_0065) and erythrose 4-phospate (E4P, stemming from the pentose phosphate pathway) (r_0042). A previous study using metabolic flux analysis showed only 8% of PEP flows divert to the shikimate pathway, and the E4P flux is ten times less than PEP (Suástegui et al., 2016). Thus, the low amount of carbon flux coupled with the imbalance between PEP and E4P stifles the production of PEA. The model predicted Uvaferm and Opale strains having more significant flux through the oxidative pentose phosphate pathway (Fig. 3, r_0091 and r_0889) partly redirected toward glycolysis. In contrast, the Elixir and R2 strains were simulated to have glycolytic flux (Fig. 3A, r_0984), being shifted toward the nonoxidative PPP. The overall PEA production values among the strains reflect these differences in routes.

Acetate ester formation is dependent on intracellular metabolic acetyl-CoA/CoA levels

Esters are a class of compounds that imbue a range of desirable fruity and floral aromas to wines and beer (Hirst and Richter, 2016). These esters are produced by a condensation reaction between acetyl or acyl-CoA and an alcohol (Saerens et al., 2010). Two types of esters are synthesized, acetate esters and fatty acid ethyl esters, respectively, based on whether acetyl- CoA or acyl-CoA is employed when forming them (Dzialo et al., 2017). More specifically, acetate esters are synthesized via the condensation of higher alcohols with acetyl-CoA, catalyzed by alcohol acetyltransferase enzymes (AATs) (Mason and Dufour, 2000). Acetate esters, primarily ethyl acetate, isoamyl acetate, isobutyl acetate, and 2-phenylethyl acetate, are quantitatively the most abundant type of esters formed during fermentation.

Our modeling analysis illustrated that acetate ester production was predominately modulated by the shifting of the acetyl-CoA/CoA ratios as the yeast cells transitioned from the exponential to the carbohydrate accumulation phase. This reflection was seen most strikingly from examining reactions associated with acetyl-CoA synthetase, alcohol acetyltransferase, malate synthase, and serine O-acetyltransferase (*ACS*s, *ATF*s, *MS*, and *SAT* related to reactions: r_0112, r_0113, r_0158 - r_0162, r_0716, and r_0992) where the strains that maintained the highest flux ratios between phases, produced the most acetate esters.

For instance, during the exponential phase, the model predicted a significant flux from isoamylol to isoamyl acetate inside the cytoplasm (6.5×10^{-5}, 5.3×10^{-5}, 6.5×10^{-5}, and 6.8×10^{-5} mmol/mmolH for Opale, R2, Elixir, and Uvaferm respectively; Fig. 4.; r_0160). This reaction sustained the same fluxes for all the strains during the carbohydrate accumulation phase. The same behavior was also observed in other ATF-associated reactions. In this reaction, acetyl-CoA is consumed to form CoA, thereby illustrating strains with higher flux ratios of acetyl-CoA/CoA were superior in producing higher acetate ester fluxes. This simulation result has been previously explored experimentally by Hong and co-workers. They showed that acetate ester formation in yeast is modulated by changing the CoA and acetyl-CoA levels by deleting and overexpressing the *BAP2* and *ATF1*genes, respectively (Hong et al., 2019). Furthermore, it has been shown that commercial yeast strains differ in the production of acetate esters, even under identical fermentation conditions, by orders of magnitude (Steensels et al., 2014). Thus, optimizing the activity of genes responsible for regulating acetyl-CoA/CoA could be beneficial in obtaining the appropriate acetate ester yield. For example, a researcher could adapt a platform tuning the enzyme expression of acetyl-CoA carboxylases for acetate esters, similar to a recent study for improving

supplies of acetyl CoA and NADPH and eventual production of 3-hydroxypropionicacid (Qin et al., 2020).

The formation of ethyl esters facilitates the removal of toxic fatty acids from cells using CoA

Although there is much certainty regarding the mechanisms that form acetate esters during fermentation, the mechanisms, including genetics and regulation of fatty acid ester formation, are still less clear. However, during the late exponential growth phase, MCFA intermediates are prematurely released from the cytoplasmic fatty acid synthase (*FAS*) complex. This release triggers ester synthesis (Taylor and Kirsop, 1977). Subsequently, CoA can activate an MCFA in combination with ATP and ethanol to enzymatically form an MCFA-ethyl ester (Saerens et al., 2010) (Fig. 4). This elaborate relationship causes the levels of fatty acid esters to depend significantly on lipid metabolism and acetyl-CoA. Some essential MCFA ethyl esters found in wines are ethyl butanoate and ethyl hexanoate.

Several investigations indicate at least three modulating routes for the flow of MCFAs to produce ethyl esters. Firstly, the upregulation of fatty acid synthases (*FAS1* and *FAS2*) and acyltransferases (*EEB1* and *EHT1*) (Saerens et al., 2010). Secondly, reduced acetyl-CoA carboxylase activity has been shown to play a role where the inhibition of acetyl-CoA carboxylase facilitates the discharge of MCFAs from the *FAS* complex (Hirst and Richter, 2016). Thirdly, an increase in MCFA concentrations induces higher concentrations of ethyl esters in wine (Saerens et al., 2008).

Here, it was shown the model is in line with the hypothesis that these three routes play a significant factor in producing MCFA ethyl esters. Higher fluxes during the exponential and carbohydrate accumulation phases in reactions associated with fatty-acyl-CoA synthase (n-C16:0CoA), fatty-acyl-CoA synthase (n-C18:0CoA), alcohol acyltransferase (butyryl-CoA), and

alcohol acyltransferase (hexanoyl-CoA) (r_2140, r_2141, r_4631, and r_4629) resulted in the higher overall production of ethyl butanoate and ethyl hexanoate for the Uvaferm and Opale strains (Fig. 4 and 5). For instance, Uvaferm and Opale experienced 71.1% and 12.6%, respectively, more flux than the Elixir strain for the reaction associated with fatty-acyl-CoA synthase (n-C16:0CoA), which resulted in 14.4% and 8.2% more overall production for Uvaferm and Opale, respectively, than the Elixir strain. Conversely, when examining the effect of acetyl-CoA carboxylase, the strain (R2) that experienced the lowest flux value for an acetyl-CoA carboxylase associated reaction (r_0109) during the exponential phase showed the highest flux for the formation of ethyl butanoate during the carbohydrate accumulation phase (6×10^{-6} mmol/mmolH, r_4646).

Lastly, by observing the intracellular fluxes related to the production and consumption of CoA, a relationship was determined (Fig, 5). For instance, we could see that there was an uptick or higher flux in ethyl esters for the strains that experienced more significant imbalances of CoA and acetyl-CoA (based on greater flux values in the direction of acetyl-CoA consumption). After evaluating the difference in CoA and acetyl-CoA producing/consuming reactions, it was determined that the Uvaferm strain had the most significant disparity. This result aligns with the prediction of the Uvaferm strain producing the most ethyl butanoate (Fig. 4). This detected mechanism for yeast to produce MCFA ethyl esters to correct imbalances of CoA and acetyl-CoA has been hypothesized before (Lambrechts and Pretorius, 2000). However, here we show that metabolic modeling supports this view. Also, since MCFAs are toxic to yeast and at sufficient concentrations can lead to stuck or sluggish fermentations (Viegas et al., 1989), strains better at producing ethyl esters from CoA are predicted to achieve a fitness advantage.

EXPERIMENTAL PROCEDURES

Experimental data

The experimental data for this study come from a previously described study published by Scott and coworkers (Scott et al., 2021a). The yeast strains used in experiments were Uvaferm 43™(Uvaferm), Lalvin R2™ (R2), Lalvin ICV Opale™ (Opale), and Vitilevure™ Elixir Yseo (Elixir), which are all commercial strains developed by Lallemand (Lallemand, Montreal, Quebec). All yeast strains were acquired from the UC Davis Enology Culture Collection. These yeast strains were selected based on their different fermentation and aroma-producing performance attributes. Furthermore, the manufacturers present qualitative characterizations of these strains, but publish information that lacks quantitative distinctions (see Table 1).

Table 1. Main enological properties of select yeast strains

Commercial Name	Species	Producer	Wine Attributes
Uvaferm 43™	*Saccharomyces cerevisiae var. bayanus*	Lallemand	Restarts stuck fermentations, neutral sensory impact, low volatile acid production
Lalvin R2™	*Saccharomyces cerevisiae var. bayanus*	Lallemand	Improves secondary aroma which leads to generating fruity and floral aroma precursors and fermentation esters.
Lalvin ICV Opale™	*Saccharomyces cerevisiae var. cerevisiae*	Lallemand	Develops more volatile aromatic compounds, resulting in intense and complex fruit aromas
Vitilevure™ Elixir Yseo	*Saccharomyces cerevisiae var. cerevisiae*	Lallemand	Spurs a vigorous production of fruity and floral aromas from esters

Genome-scale metabolic model (GEM)

The GEM used in this study was *Yeast8.5.0* (Lu et al., 2019), publicly available on GitHub (see link: https://github.com/SysBioChalmers/yeast-GEM). The GEM contains 2742 metabolites, 4058 reactions, and 1150 genes. The GEM was initially developed for *S. cerevisiae* S288C, a haploid laboratory strain that is not employed in winemaking. However, since this study was applied to fermentations under enological conditions, we modified the GEM to appropriately reflect the anaerobic state of metabolism. In our approach, we proceeded as suggested by Heavner and coworkers (Heavner et al., 2013), constraining v_{O_2} to zero (LB=UB=0 [mmol/g DW h]), allowing unrestricted uptake of ergosterol (r_1757), lanosterol (r_1915), zymosterol (r_2106), 14-

demethyllanosterol (r_2134), and ergosta-5,7,22,24(28)-tetraen-3beta-ol (r_2137) and oleate (r_2189). In addition, pathways including the oxaloacetate-malate shuttle and glycerol dehydrogenase reaction were unrestricted as described by Sanchez and coworkers (Sánchez et al., 2017, Sánchez et al., 2019) (in the model, this was achieved by blocking reactions r_0713, r_0714, and r_0487). Heme A was also removed from the not used under anaerobic conditions. All the changes related to anaerobiosis were applied either at the beginning of the fermentation or after the depletion of the initially dissolved oxygen in the simulated media. Moreover, *Yeast8.5.0* includes expanded coverage of aroma-associated pathways such as an extended Ehrlich pathway, more ester formation reactions, and enhanced sulfur reduction pathways as previously performed and described in the literature (Scott et al., 2020).

Flux balance analysis

Flux balance analysis (FBA) (Varma and Palsson, 1994, Orth et al., 2010) is a modeling framework based on knowledge of reaction stoichiometry and mass/charge balances. The framework relies on the pseudo-steady-state assumption (no intracellular accumulation of metabolites occurs). The well-known expression captures FBA:

$$\mathbf{S} \cdot \mathbf{v} = \mathbf{0}$$

where **S** is the stoichiometric matrix of (*n* metabolites by *m* reactions), and **b** is a vector of metabolic fluxes. The number of unknown fluxes is higher than the number of equations, and thus the system is undetermined. Still, it is possible to find a unique solution under the assumption that cell metabolism evolves to pursue a predetermined goal which is defined as the maximization (or minimization) of a particular objective function (J):

$$\max J$$

$$s.t.: \quad \mathbf{S} \cdot \mathbf{v} = \mathbf{0}$$

$$\mathbf{LB} < \mathbf{v} < \mathbf{UB}$$

where **LB** and **UB** correspond to the lower and upper bounds on the estimated fluxes. Examples of objective functions J include growth rate, ATP, or the negative of nutrient consumption, etc.

Typically, there are multiple optimal solutions for a given FBA problem. The result in parsimonious FBA (pFBA) is the most parsimonious of the optimal solutions, i.e., the solution that achieves the specific objective with the minimal use of gene products and the minimization of the total flux load (Machado et al., 2014).

Parameter estimation.

Parameter estimation aims to compute the unknown parameters - growth-related constants and kinetic parameters - that minimize some measure of the distance between the data and the model predictions. The maximum-likelihood principle yields an appropriate measure of such a distance (Walter and Pronzato, 1997):

$$J_{mc}(\theta\theta) = \sum_{k=1}^{n_{exp}} \sum_{j=1}^{n_{obs}} \sum_{i=1}^{n_{st}} \left(\frac{y_{k,j,i}(\theta\theta) - y_{k,j,i}^{m}}{\sigma_{k,j,i}} \right)^2,$$

where n_{exp}, n_{obs} and $n_{st}$are, respectively, the number of experiments, observables (measured quantities), and sampling times while $\sigma_{k,j,i}$ represents the standard deviation of the measured data as obtained from the experimental replicates. $y_{k,j,i}^{m}$ represents each of the measured quantities, $y_{k,j,i}^{m}$ and C^m in our case, and $y_{k,j,i}(\theta\theta)$ corresponds to model predicted values, X and C.

Observation functions were included for CFUs and OD_{600} was included to scale viable cell-mass (X_V) and active cell-mass (X_A), respectively.

Parameters are estimated by solving a nonlinear optimization problem where the aim is to find the unknown parameter values (θ) to minimize $J_{mc}(\theta\theta)$ subject to the system dynamics - the model- and parameter bounds (Balsa-Canto et al., 2010). Analysis of dynamic metabolic fluxes.

Computing Environment

The modeling was performed in MATLAB® 2020b (The MathWorks, Inc., Cambridge, MA, USA) using Cobra Toolbox 3.0 (Heirendt et al., 2019) and implemented on a Windows 10 (Microsoft Corporation, Redmond, WA, USA) Intel® (Intel Corporation, Santa Clara, CA, USA) Core™ i7-7500 CPU @ 2.70 GHz–2.90 GHz processor. The GEM was imported into MATLAB as an SBML file and curated using Cobra Toolbox. Git version 2.3.0 was installed before cloning COBRA with GitHub and initializing COBRA in MATLAB.

The multi-phase multi-objective genome-scale model was implemented as a script for AMIGO2 toolbox (Balsa-Canto et al., 2016) to facilitate parameter estimation, simulation, and quality of fit analyses.

ACKNOWLEDGEMENTS

E. B-C. acknowledges funding from MCIU/AEI/FEDER, UE (grant reference: RTI2018-093744-B-C33), and Xunta de Galicia (IN607B 2020/03). In addition, some materials and resources were funded by a Wageningen University and Research internal fund from the Food Microbiology department.

***Authors' contributions*: CRediT (Contribution Roles Taxonomy)-** Conceptualization, W.T.S.J., D.H, E.J.S., R.A.N., and E.B-C.; Data Curation, W.T.S.J. and D.H., Formal Analysis, W.T.S.J., D.H., and E.B-C.; Funding Acquisition, E.J.S. and E.B-C; Investigation, W.T.S.J.; Methodology, W.T.S.J., D.H., and E.B-C.; Resources, R.A.N, and E.B-C.; Software, D.H, and E.B-C.; Supervision, E.J.S, R.A.N., and E.B-C.; Validation, W.T.S.J.; Visualization, W.T.S.J., D.H., and E.B-C; Writing—original draft, W.T.S.J.; Writing—review and editing, W.T.S.J., D.H., E.J.S., R.A.N., and E.B-C. All authors have read and agreed to the published version of the manuscript.

CONFLICT OF INTEREST

The authors declare no competing interests

FIGURE CAPTIONS

Figure 1. Details on the implementation of the multi-phase and multi-objective dynamic genome-scale model to simulate batch fermentation. Multi-phase and multi-objective dynamic FBA and methodology to compute dynamic flux rates. The process starts at t_0 ¼ 0 and ends at t_F; the timing of each phase t_L, t_E, t_S, and t_D is computed through parameter estimation.

Figure 2. Overview of central carbon metabolism. Panels a to f depict model predictions versus the experimental data on extracellular metabolite concentrations associated with glycolysis and central carbon metabolism for the four strains. Panel g illustrates the predicted intracellular dynamic flux ratios during the carbohydrate accumulation phase, showing how the four commercial strains employ different redox balance strategies. These differences result in the differential production of relevant external metabolites such as succinate (a), glycerol (d), ethanol (e), and acetate (f).

Figure 3. Overview of higher-alcohol production. Panel a depicts the predicted intracellular flux dynamic flux ratios related to higher alcohols: propanol, 2-phenylethanol (PEA), isobutanol, and isoamylol during the carbohydrate accumulation phase and their related effect on the redox balance of cofactors. Panels b to f represent a comparison between model predictions and experimental values of PEA, threonine, propanol, isobutanol, and isoamylol, respectively.

Figure 4. Overview of acetate and fatty acid ethyl ester production. Panel a shows the predicted intracellular dynamic flux ratios corresponding to the production of esters: 2-phenylethyl acetate, isoamyl acetate, ethyl acetate, and ethyl butanoate during the carbohydrate accumulation phase and their respective impact on the cofactor balance. Panels b to i correspond to the comparison between model predictions and experimental data of 2-phenylethyl acetate, isoamyl acetate, ethyl acetate, ethyl butanoate, respectively.

Figure 5. Comparative illustration of the fluxes through the reactions consuming and producing acetyl-CoA during the carbohydrate accumulation phase, illustrating how acetyl-CoA/CoA ratios modulate cellular phenotype.

REFERENCES.

Albers, E., Larsson, C., Lidén, G., Niklasson, C., and Gustafsson, L. (1996) Influence of the nitrogen source on *Saccharomyces cerevisiae* anaerobic growth and product formation, *Appl. Environ. Microbiol.* **62**: 3187-3195.

Aung, H.W., Henry, S.A., and Walker, L.P. (2013) Revising the representation of fatty acid, glycerolipid, and glycerophospholipid metabolism in the consensus model of yeast metabolism, *Ind. Biotechnol.* **9**: 215-228.

Balsa-Canto, E., Alonso, A.A., and Banga, J.R. (2010) An iterative identification procedure for dynamic modeling of biochemical networks, *BMC Syst. Biol.* **4**: 11.

Balsa-Canto, E., Henriques, D., Gábor, A., and Banga, J.R. (2016) AMIGO2, a toolbox for dynamic modeling, optimization and control in systems biology, *Bioinformatics* **32**: 3357-3359.

Botstein, D., Chervitz, S.A., and Cherry, M. (1997) Yeast as a model organism, *Science* **277**: 1259-1260.

Boulton, R. (1980) The prediction of fermentation behavior by a kinetic model, *Am. J. Enol. Vitic.* **31**: 40.

Cramer, A.C., Vlassides, S., and Block, D.E. (2002) Kinetic model for nitrogen-limited wine fermentations, *Biotechnol. Bioeng.* **77**: 49-60.

Crépin, L., Truong, N.M., Bloem, A., Sanchez, I., Dequin, S., and Camarasa, C. (2017) Management of multiple nitrogen sources during wine fermentation by *Saccharomyces cerevisiae*, *Appl. Environ. Microbiol.* **83**: e02617-02616.

Dekoninck, T. (2012) Bottle conditioning of beer strategies to improve yeast refermentation performance.

Dunn, B., Levine, R.P., and Sherlock, G. (2005) Microarray karyotyping of commercial wine yeast strains reveals shared, as well as unique, genomic signatures, *BMC Genomics* **6**: 53.

Dzialo, M.C., Park, R., Steensels, J., Lievens, B., and Verstrepen, K.J. (2017) Physiology, ecology and industrial applications of aroma formation in yeast, *FEMS Microbiol. Rev.* **41**: S95-S128.

Ehrlich, F. (1907) Über die Bedingungen der Fuselölbildung und über ihren Zusammenhang mit dem Eiweissaufbau der Hefe, *Berichte der deutschen chemischen Gesellschaft* **40**: 1027-1047.

Forster, J., Famili, I., Fu, P., Palsson, B.O., and Nielsen, J. (2003) Genome-scale reconstruction of the *Saccharomyces cerevisiae* metabolic network, *Genome Research* **13**: 244-253.

Gonzalez, R., and Morales, P. (2017) Wine secondary aroma: understanding yeast production of higher alcohols, *Microb. Biotechnol.* **10**: 1449-1450.

Hazelwood, L.A., Daran, J.-M., van Maris, A.J.A., Pronk, J.T., and Dickinson, J.R. (2008) The Ehrlich pathway for fusel alcohol production: a century of research on *Saccharomyces cerevisiae* metabolism, *Appl. Environ. Microbiol.* **74**: 2259-2266.

Heavner, B.D., Smallbone, K., Price, N.D., and Walker, L.P. (2013) Version 6 of the consensus yeast metabolic network refines biochemical coverage and improves model performance, *Database* **2013**.

Heirendt, L., Arreckx, S., Pfau, T., Mendoza, S.N., Richelle, A., Heinken, A., et al. (2019) Creation and analysis of biochemical constraint-based models using the COBRA Toolbox v.3.0, *Nature Protocols* **14**: 639-702.

Henderson, C.M., Lozada-Contreras, M., Jiranek, V., Longo, M.L., and Block, D.E. (2013) Ethanol production and maximum cell growth are highly correlated with membrane lipid composition during fermentation as determined by lipidomic analysis of 22 *Saccharomyces cerevisiae* strains, *Appl. Environ. Microbiol.* **79**: 91-104.

Henriques, D., Balsa-Canto, E., and Druzhinina, I.S. (2021a) The Monod model is insufficient to explain biomass growth in nitrogen-limited yeast fermentation, *Applied and Environmental Microbiology* **87**: e01084-01021.

Henriques, D., Minebois, R., Mendoza, S.N., Macías, L.G., Pérez-Torrado, R., Barrio, E., et al. (2021b) A multi-phase multi-objective dynamic genome-scale model shows different redox balancing among yeast species of the *Saccharomyces* genus in fermentation, *mSystems* **6**: e00260-00221.

Hirst, M.B., and Richter, C.L. (2016) Review of aroma formation through metabolic pathways of *Saccharomyces cerevisiae* in beverage fermentations, *Am. J. Enol. Vitic.* **67**: 361-370.

Hong, K.-Q., Fu, X.-M., Dong, S.-S., Xiao, D.-g., and Dong, J. (2019) Modulating acetate ester and higher alcohol production in *Saccharomyces cerevisiae* through the cofactor engineering, *J. Ind. Microbiol. Biotechnol.* **46**: 1003-1011.

Ingledew, W., and Kunkee, R.E. (1985) Factors influencing sluggish fermentations of grape juice, *Am. J. Enol. Vitic.* **36**: 65-76.

Jain, V.K., Divol, B., Prior, B.A., and Bauer, F.F. (2012) Effect of alternative NAD+-regenerating pathways on the formation of primary and secondary aroma compounds in a *Saccharomyces cerevisiae* glycerol-defective mutant, *Appl. Microbiol. Biotechnol.* **93**: 131-141.

Lam, F.H., Ghaderi, A., Fink, G.R., and Stephanopoulos, G. (2014) Engineering alcohol tolerance in yeast, *Science* **346**: 71-75.

Lambrechts, M., and Pretorius, I. (2000) Yeast and its importance to wine aroma-a review, *S. Afr. J. Enol. Vitic* **21**: 97-129.

Lu, H., Li, F., Sanchez, B.J., Zhu, Z., Li, G., Domenzain, I., et al. (2019) A consensus *S. cerevisiae* metabolic model Yeast8 and its ecosystem for comprehensively probing cellular metabolism, *Nature Communications* **10**: 3586.

Machado, D., Rodrigues, L.R., and Rocha, I. (2014) A kinetic model for curcumin production in *Escherichia coli*, *Biosystems* **125**: 16-21.

Mason, A.B., and Dufour, J.-P. (2000) Alcohol acetyltransferases and the significance of ester synthesis in yeast, *Yeast* **16**: 1287-1298.

Miller, A.C., Wolff, S.R., Bisson, L.F., and Ebeler, S.E. (2007) Yeast strain and nitrogen supplementation: Dynamics of volatile ester production in Chardonnay juice fermentations, *Am. J. Enol. Vitic.* **58**: 470-483.

Moreno-Paz, S., Schmitz, J., Martins dos Santos, V.A.P., and Suarez-Diez, M. (2022) Enzyme-constrained models predict the dynamics of *Saccharomyces cerevisiae* growth in continuous, batch and fed-batch bioreactors, *Microb. Biotechnol.* **n/a**.

Nisbet, M.A., Tobias, H.J., Brenna, J.T., Sacks, G.L., and Mansfield, A.K. (2014) Quantifying the contribution of grape hexoses to wine volatiles by high-precision [U13C]-glucose tracer studies, *J. Agric. Food. Chem.* **62**: 6820-6827.

Nissen, T.L., Schulze, U., Nielsen, J., and Villadsen, J. (1997) Flux distributions in anaerobic, glucose-limited continuous cultures of *Saccharomyces cerevisiae*, *Microbiology* **143**: 203-218.

Nookaew, I., Jewett, M.C., Meechai, A., Thammarongtham, C., Laoteng, K., Cheevadhanarak, S., et al. (2008) The genome-scale metabolic model iIN800 of *Saccharomyces cerevisiae* and its validation: a scaffold to query lipid metabolism, *BMC Syst. Biol.* **2**: 71.

Orth, J.D., Thiele, I., and Palsson, B.O. (2010) What is flux balance analysis?, *Nature Biotechnology* **28**: 245-248.

Pérez, D., Jaehde, I., Guillamón, J.M., Heras, J.M., and Querol, A. (2021) Screening of *Saccharomyces* strains for the capacity to produce desirable fermentative compounds under the influence of different nitrogen sources in synthetic wine fermentations, *Food Microbiol.* **97**: 103763.

Peter, J., De Chiara, M., Friedrich, A., Yue, J.X., Pflieger, D., Bergstrom, A., et al. (2018) Genome evolution across 1,011 *Saccharomyces cerevisiae* isolates, *Nature* **556**: 339-344.

Pizarro, F., Varela, C., Martabit, C., Bruno, C., Prez-Correa, J.R., and Agosin, E. (2007) Coupling kinetic expressions and metabolic networks for predicting wine fermentations, *Biotechnol. Bioeng.* **98**: 986-998.

Qin, N., Li, L., Ji, X., Li, X., Zhang, Y., Larsson, C., et al. (2020) Rewiring Central Carbon Metabolism Ensures Increased Provision of Acetyl-CoA and NADPH Required for 3-OH-Propionic Acid Production, *ACS Synthetic Biology* **9**: 3236-3244.

Quiros, M., Martinez-Moreno, R., Albiol, J., Morales, P., Vazquez-Lima, F., Barreiro-Vazquez, A., et al. (2013) Metabolic flux analysis during the exponential growth phase of *Saccharomyces cerevisiae* in wine fermentations, *PLoS One* **8**: e71909.

Ribéreau-Gayon, P., Dubourdieu, D., Doneche, B., and Lonvaud, A. (2000) Biochemistry of alcoholic fermentation and metabolic pathways of wine yeasts, *Handbook of Enology Volume* **1**: 51-74.

Rollero, S., Bloem, A., Camarasa, C., Sanchez, I., Ortiz-Julien, A., Sablayrolles, J.-M., et al. (2015) Combined effects of nutrients and temperature on the production of fermentative aromas by *Saccharomyces cerevisiae* during wine fermentation, *Appl. Microbiol. Biotechnol.* **99**: 2291-2304.

Rossouw, D., Næs, T., and Bauer, F.F. (2008) Linking gene regulation and the exo-metabolome: A comparative transcriptomics approach to identify genes that impact on the production of volatile aroma compounds in yeast, *BMC Genomics* **9**: 530.

Saerens, S., Delvaux, F., Verstrepen, K., Van Dijck, P., Thevelein, J., and Delvaux, F. (2008) Parameters affecting ethyl ester production by *Saccharomyces cerevisiae* during fermentation, *Appl. Environ. Microbiol.* **74**: 454-461.

Saerens, S.M.G., Delvaux, F.R., Verstrepen, K.J., and Thevelein, J.M. (2010) Production and biological function of volatile esters in *Saccharomyces cerevisiae*, *Microb. Biotechnol.* **3**: 165-177.

Sainz, J., Pizarro, F., Pérez-Correa, J.R., and Agosin, E. (2003) Modeling of yeast metabolism and process dynamics in batch fermentation, *Biotechnol. Bioeng.* **81**: 818-828.

Sánchez, B.J., Li, F., Kerkhoven, E.J., and Nielsen, J. (2019) SLIMEr: probing flexibility of lipid metabolism in yeast with an improved constraint-based modeling framework, *BMC Syst. Biol.* **13**: 4.

Sánchez, B.J., Zhang, C., Nilsson, A., Lahtvee, P.-J., Kerkhoven, E.J., and Nielsen, J. (2017) Improving the phenotype predictions of a yeast genome-scale metabolic model by incorporating enzymatic constraints, *Molecular Systems Biology* **13**: 935.

Scott, W.T., Mastrigt, O.v., Block, D.E., Notebaart, R.A., Smid, E.J., and Cuomo, C.A. (2021a) Nitrogenous Compound Utilization and Production of Volatile Organic Compounds among Commercial Wine Yeasts Highlight Strain-Specific Metabolic Diversity, *Microbiology Spectrum* **9**: e00485-00421.

Scott, W.T., Smid, E.J., Block, D.E., and Notebaart, R.A. (2021b) Metabolic flux sampling predicts strain-dependent differences related to aroma production among commercial wine yeasts, *Microb. Cell Fact.* **20**: 204.

Scott, W.T., Smid, E.J., Notebaart, R.A., and Block, D.E. (2020) Curation and analysis of a *Saccharomyces cerevisiae* genome-scale metabolic model for predicting production of sensory impact molecules under enological conditions, *Processes* **8**: 1195.

Seguinot, P., Rollero, S., Sanchez, I., Sablayrolles, J.-M., Ortiz-Julien, A., Camarasa, C., and Mouret, J.-R. (2018) Impact of the timing and the nature of nitrogen additions on the production kinetics of fermentative aromas by *Saccharomyces cerevisiae* during winemaking fermentation in synthetic media, *Food Microbiol.* **76**: 29-39.

Snoek, T., Verstrepen, K.J., and Voordeckers, K. (2016) How do yeast cells become tolerant to high ethanol concentrations?, *Curr. Genet.* **62**: 475-480.

Steensels, J., Meersman, E., Snoek, T., Saels, V., Verstrepen, K.J., and Cullen, D. (2014) Large-scale selection and breeding To generate industrial yeasts with superior aroma production, *Applied and Environmental Microbiology* **80**: 6965-6975.

Su, Y., Heras, J.M., Gamero, A., Querol, A., and Guillamón, J.M. (2021) Impact of nitrogen addition on wine fermentation by *S. cerevisiae* strains with different nitrogen requirements, *J. Agric. Food. Chem.* **69**: 6022-6031.

Suástegui, M., Guo, W., Feng, X., and Shao, Z. (2016) Investigating strain dependency in the production of aromatic compounds in *Saccharomyces cerevisiae*, *Biotechnol. Bioeng.* **113**: 2676-2685.

Taylor, G.T., and Kirsop, B.H. (1977) The origin of the medium-chain length fatty acids present in beer, *J. Inst. Brew.* **83**: 241-243.

Tesnière, C., Brice, C., and Blondin, B. (2015) Responses of *Saccharomyces cerevisiae* to nitrogen starvation in wine alcoholic fermentation, *Appl. Microbiol. Biotechnol.* **99**: 7025-7034.

Varela, C., Pizarro, F., and Agosin, E. (2004) Biomass content governs fermentation rate in nitrogen-deficient wine musts, *Appl. Environ. Microbiol.* **70**: 3392-3400.

Vargas, F.A., Pizarro, F., Pérez-Correa, J.R., and Agosin, E. (2011) Expanding a dynamic flux balance model of yeast fermentation to genome-scale, *BMC Syst. Biol.* **5**: 75.

Varma, A., and Palsson, B.O. (1994) Stoichiometric flux balance models quantitatively predict growth and metabolic by-product secretion in wild-type *Escherichia coli W3110*, *Applied and Environmental Microbiology* **60**: 3724-3731.

Viegas, C.A., Rosa, M.F., Sá-Correia, I., and Novais, J.M. (1989) Inhibition of yeast growth by octanoic and decanoic acids produced during ethanolic fermentation, *Applied and Environmental Microbiology* **55**: 21-28.

Walter, E., and Pronzato, L. (1997) *Identification of parametric models from experimental data*. Berlin; New York; Paris: Springer ; Masson.

Phases, objectives and dynamic flux ratios

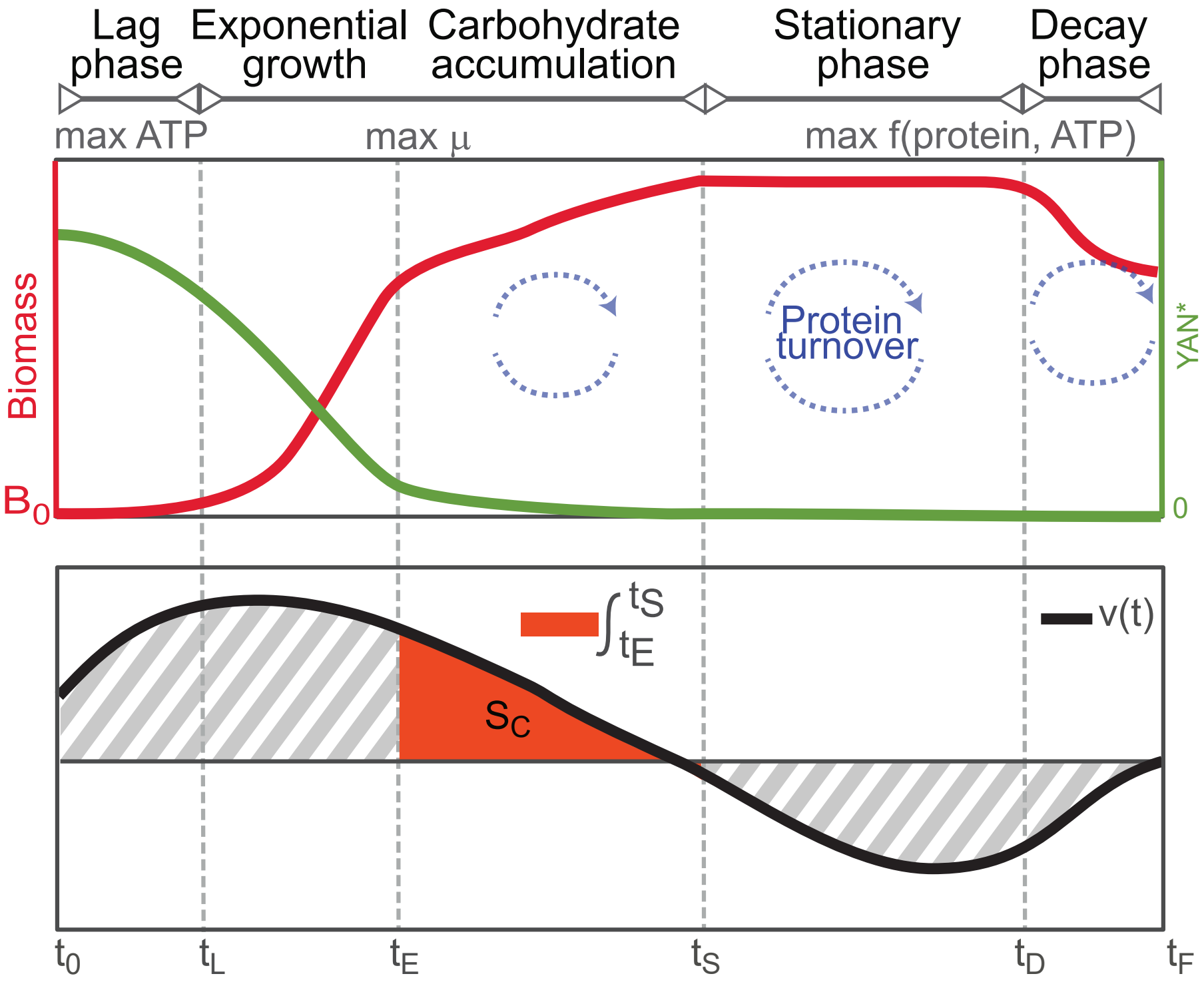

Predicted dynamic flux ratios

Central carbon metabolism

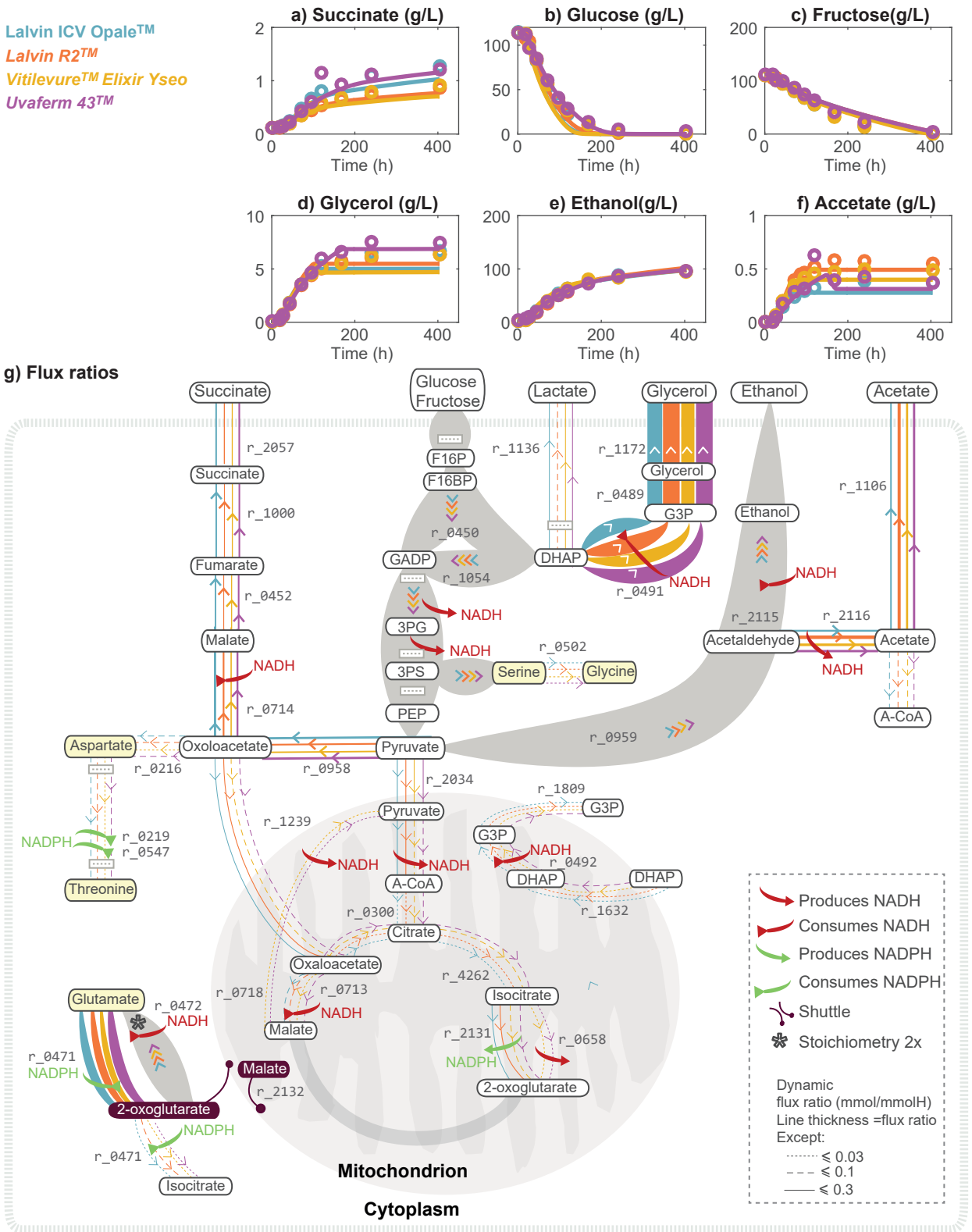

Production of higher alcohols

a) Flux ratios

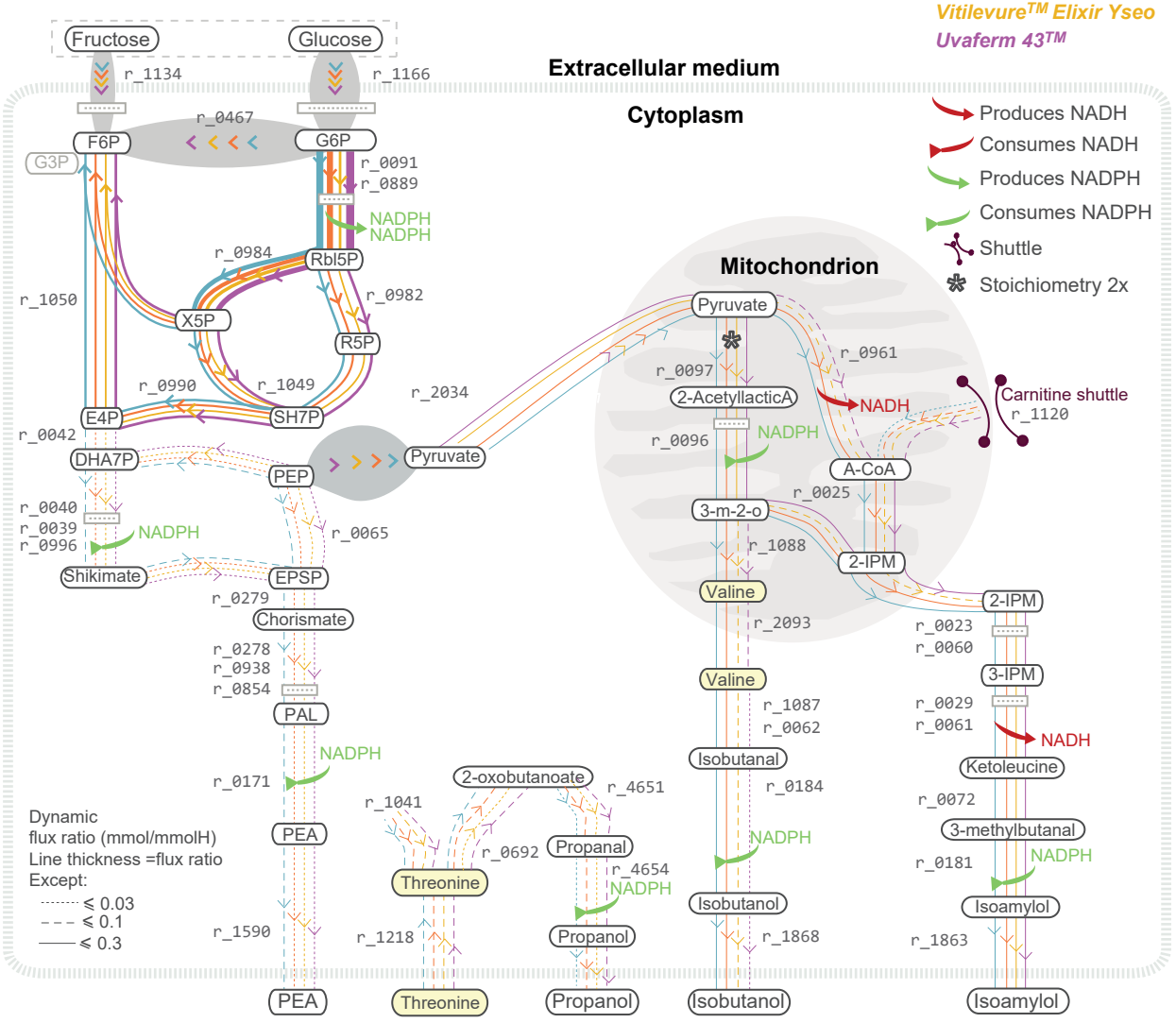

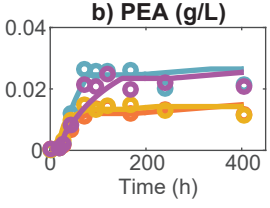

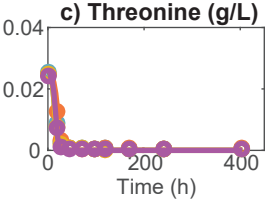

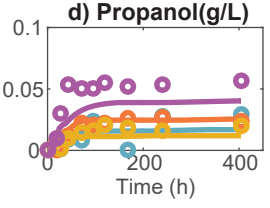

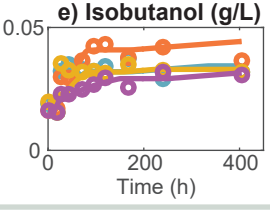

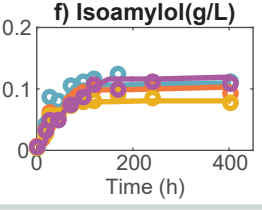

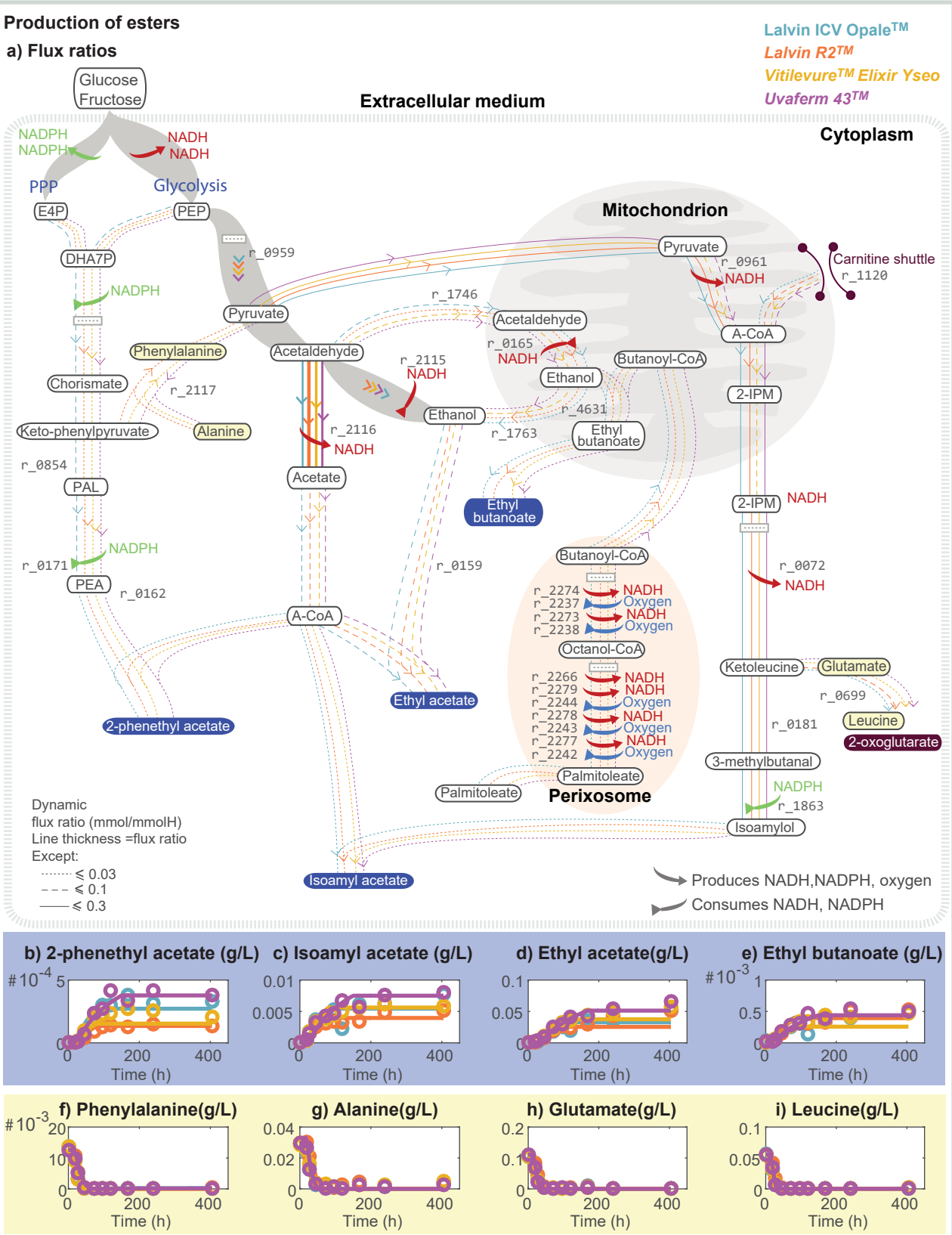
Production of esters
a) Flux ratios
Lalvin ICV Opale™
Lalvin R2™
Vitilevure™ Elixir Yseo
Uvaferm 43™
Extracellular medium
Cytoplasm
Mitochondrion
Perixosome
Glucose
Fructose
NADPH
NADPH
NADH
NADH
PPP
Glycolysis
E4P
PEP
DHA7P
r_0959
Pyruvate
Phenylalanine
Acetaldehyde
Chorismate
r_2117
Keto-phenylpyruvate
Alanine
r_0854
PAL
r_0171
PEA
r_0162
r_2115
r_2116
Acetate
A-CoA
r_1746
r_0165
Ethanol
r_4631
r_1763
Ethyl butanoate
r_0159
Ethyl acetate
2-phenethyl acetate
Isoamyl acetate
Butanoyl-CoA
r_2274
r_2237
r_2273
r_2238
Oxygen
Octanol-CoA
r_2266
r_2279
r_2244
r_2278
r_2243
r_2277
r_2242
Palmitoleate
Pyruvate
r_0961
Carnitine shuttle
r_1120
A-CoA
2-IPM
r_0072
Ketoleucine
Glutamate
r_0699
Leucine
2-oxoglutarate
r_0181
3-methylbutanal
r_1863
Isoamylol
Dynamic
flux ratio (mmol/mmolH)
Line thickness =flux ratio
Except:
≤ 0.03
≤ 0.1
≤ 0.3
Produces NADH,NADPH, oxygen
Consumes NADH, NADPH
b) 2-phenethyl acetate (g/L)
c) Isoamyl acetate (g/L)
d) Ethyl acetate(g/L)
e) Ethyl butanoate (g/L)
f) Phenylalanine(g/L)
g) Alanine(g/L)
h) Glutamate(g/L)
i) Leucine(g/L)
Time (h)
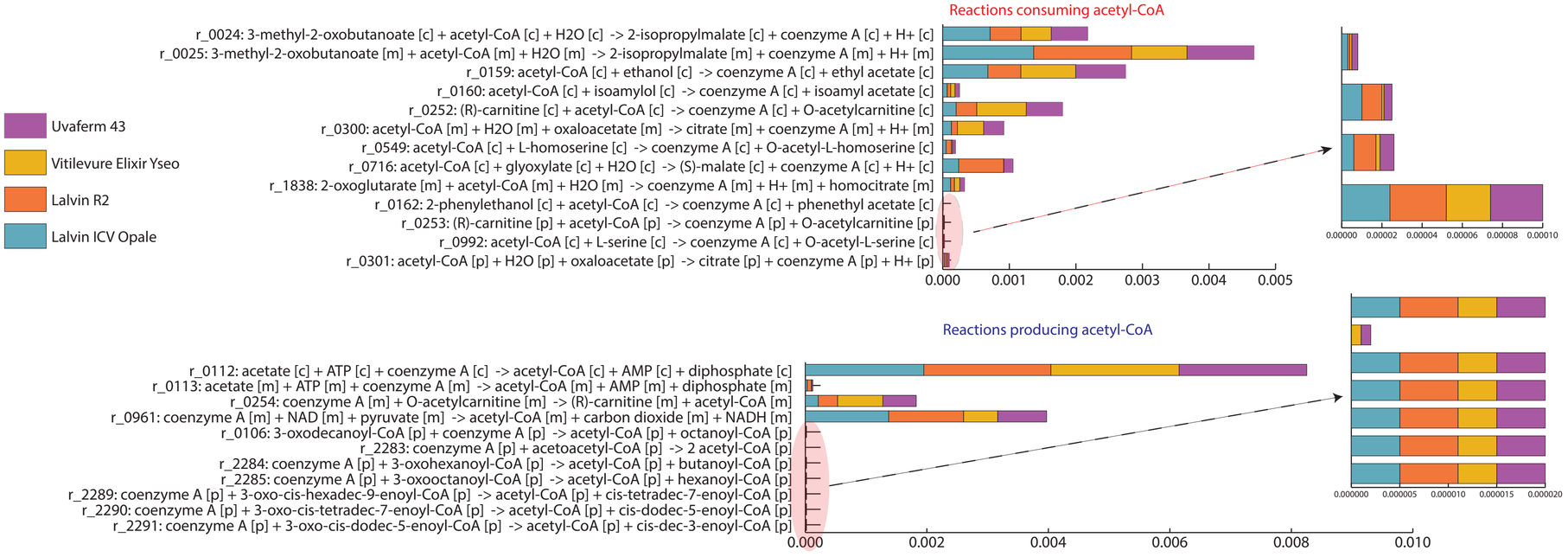
Dynamic flux ratios that contribute to cofactor (acetyl-CoA/CoA) balance